Computational Materials Science 148 (2018) 54–59

Contents lists available at ScienceDirect

Computational Materials Science

journal homepage: www.elsevier.com/locate/commatsci

Editor's Choice

The intrinsic low lattice thermal conductivity in the rock salt SnSe

Yun Xie, Yang Zhou, Xin-Gao Gong *

Key Laboratory for Computational Physical Science (Ministry of Education), State Key Laboratory of Surface Physics and Department of Physics, Fudan University, Shanghai 200433, China
Collaborative Innovation Center of Advanced Microstructures, Nanjing 210093, Jiangsu, China

ARTICLE INFO

Article history:
Received 24 December 2017
Received in revised form 18 January 2018
Accepted 20 January 2018
Available online 22 February 2018

Keywords:
The rock salt SnSe
Ab initio calculations
Boltzmann transport equation
Thermal conductivity
Thermal transport properties

ABSTRACT

The rock-salt IV-VI compounds usually have low thermal conductivity, while the orthorhombic Tin Selenide (SnSe) was reported to show extremely low lattice thermal conductivity (κ_L) and thus achieves a record high zT value. To understand why SnSe has low thermal conductivity and how important role played by the orthorhombic structure, we studied κ_L for both forms of SnSe, the rock salt and the orthorhombic, based on first-principles calculations and the Boltzmann transport equation. We found an even smaller value of κ_L for the rock salt structure, which establishes a possibility for even larger zT materials. Detailed analyses were performed on thermal properties for both structures. We attributed the low κ_L of the rock salt SnSe to its large Grüneisen parameters, which stem from the strongly anharmonic phonons. Our findings indicate the indecisive role that the orthorhombic structure is playing in achieving low κ_L for SnSe and provide fresh insight in understanding the thermal properties of SnSe.

1. Introduction

Thermoelectric (TE) materials are of great interest because of their potential to convert heat into electricity [1–5]. The efficiency of TE materials is determined by the dimensionless figure of merit $zT = S^2\sigma/K$ where S, σ, K represents the Seebeck coefficient, the electrical conductivity and the thermal conductivity, respectively. The recent report of the IV-VI compound orthorhombic SnSe achieving a record high figure of merit $zT = 2.6 \pm 0.3$ along specific crystallographic directions or $zT = 1.34$ in device form has attracted tremendous interest in the scientific community [6,7]. Usually a high zT value requires a large power factor as well as a low thermal conductivity, which are, unfortunately, difficult to be realized simultaneously in experiments. The key aspect of making the orthorhombic SnSe one of the most promising TE materials is owed to its ultra-low κ_L in the range of 300 K up to 900 K, which is lower than that of many other IV-VI TE materials [6]. This intrinsic low thermal conductivity can alleviate the complex strategies used in practice to reduceκ_L and allows more flexible procedures in improving zT as a whole. Different from many other IV-VI TE compounds (e.g. PbSe, PbTe) which adopt the higher symmetry rock salt structure [8], SnSe has the orthorhombic structure at room temperature [6,7]. The orthorhombic structure can be achieved from its rock salt counterpart with a three-dimensional distortion. In this respect they are closely related to each other.

Although the underlying thermal transport properties of orthorhombic SnSe have been investigated both theoretically and experimentally [6,7,9–17], it is so far not clear whether the orthorhombic structure is the decisive factor for SnSe to achieve such a low κ_L. A good way to find out what role the structure is playing in reducing κ_L would be examining how κ_L changes and how the thermal properties evolve if SnSe adopts the rock salt structure rather than the orthorhombic structure. This comparative study between the two structures will provide us new insight towards understanding the underlying thermal transport properties of SnSe, which plays the key role in making SnSe the highest zT TE material [6], and it will certainly be helpful for seeking new materials with better zT.

In this paper, we report comprehensive investigations into the thermal properties of the orthorhombic and the rock salt SnSe using first-principles calculations and the Boltzmann transport equation (BTE). This approach has recently been implemented in studies of orthorhombic SnSe and other IV-VI TE materials such as PbTe and PbSe [18], yielding good agreement with the experimental results. We identified an even smaller value of κ_L for the rock salt SnSe. This finding provides evidence that the orthorhombic crystal structure is an indecisive factor in achieving low κ_L for SnSe. Further analysis of the thermal properties of the two structures attributed the reduction of κ_L for the rock salt SnSe to its

* Corresponding author at: Key Laboratory for Computational Physical Science (Ministry of Education), State Key Laboratory of Surface Physics and Department of Physics, Fudan University, Shanghai 200433, China.
E-mail address: xggong@fudan.edu.cn (X.-G. Gong).

https://doi.org/10.1016/j.commatsci.2018.01.045
0927-0256/

large Grüneisen parameters, which stem from the strongly anharmonic phonons.

2. Computational methods

We employed the plane-wave basis set and the projected augmented wave method [19,20], which is implemented in the VASP code [21,22], to calculate the electronic properties. The Perdew–Burke–Ernzerhof (PBE) [23] method of generalized gradient approximation (GGA) was chosen as the exchange–correlation functional. An energy cutoff of 400 eV was adopted in all the calculations, which was tested to ensure convergence. A total energy change less that 10^{-8} was selected as the convergence criteria for structural optimization, and spin-orbit interaction (SOI) effects were considered in the band structure calculations.

Lattice-dynamics calculations were carried out using the Phonopy package [24], with VASP employed as the calculator to obtain interatomic force constants (IFCs) via a finite-displacement approach. We used the crystal cell containing 8 atoms for the thermal transport calculations of the rock salt SnSe (Fig. 1b). The thermoelectric properties of SnSe were determined by solving the Boltzmann transport equation (BTE) which was implemented in the ShengBTE [25] package. For the rock salt SnSe, a $2 \times 2 \times 2$ supercell was constructed for the second- and third-order IFC calculations, while for the orthorhombic phase we used a $2 \times 4 \times 4$ supercell.

3. Results and discussion

3.1. Lattice parameters and electronic band structures

Fig. 1 shows the lattice structure of the orthorhombic SnSe (Pnma) and the rock salt (Fm3m) SnSe, respectively. The lattice constants of the orthorhombic structure are fully relaxed to be 11.76 Å, 4.20 Å, 4.55 Å along the a, b and c directions, respectively, which is in good agreement with previous DFT calculations [9] and experimental measurements [6,7]. The orthorhombic SnSe adopts a two-atom-thick layered structure along the [1 0 0] direction at room temperature with the corrugated layers creating zig-zag and arm-chair edges along the [0 1 0] and [0 0 1] directions, respectively. The calculated lattice constant of the rock salt SnSe is 6.06 Å, a little smaller than that of PbTe (6.44) and PbSe (6.10) [26]. The orthorhombic structure contains highly distorted $SnSe_7$ (Fig. 1a) polyhedrally coordinated, with three short bonds (d_1, $2*d_2$) and four long bonds ($2*d_3$, d_4, d_5) which may be conceptualized as a distorted variation from the higher symmetry $SnSe_6$ coordination of the rock salt phase (Fig. 1b).

The electronic band structures of both structures along some high symmetry directions are plotted in Fig. 2. The orthorhombic SnSe has an indirect gap of 0.59 eV with the valence band maximum along the Γ-Z direction and the conduction band minimum along the Γ-Y direction. The band structure of the rock salt SnSe accommodates a gapless three-dimensional Dirac cone located along the L-W line as shown in Fig. 2b, the implementation of SOI opens a gap of 0.19 eV in the vicinity of the L point. The most remarkable difference between the two band structures is that the non-parabolic, complex multiband valence states of the orthorhombic SnSe are totally absent in the rock salt phase. Note that the heavy (Σ) and light (L) bands near the Fermi surface of the rock salt SnSe would be good candidates for band engineering [27], which may enhance thermoelectric performance.

3.2. Lattice thermal conductivities and thermal transport properties

The optical phonon modes of the rock salt SnSe have generally lower energies than that those of the orthorhombic structure. Fig. 3 shows the computed phonon dispersions and phonon vibrational density of states (VDOS) for both structures. The phonon spectrum of the original rock salt SnSe structure shows three degenerate imaginary optical phonons at Gamma point with the value around −0.7 THz. Here we adopt a small structural modulation of the Se sub-lattice off-centered along (1 1 1) direction by ~0.1 Å to the rock salt phase to eliminate the imaginary frequency which we believe has little effect to the thermal properties. There are 3 acoustic and 21 optical phonon branches for each structure, corresponds to 8 atoms per unit cell. Although the phonon frequencies in the acoustic region of the two phases are comparable with each other, the phonon frequencies of the optical modes of the rock salt SnSe are smaller compared to those in orthorhombic SnSe. This can be qualitatively understood considering the distortion from the $SnSe_6$ coordination (Fig. 1b) to the $SnSe_7$ coordination (Fig. 1a) where both the shorter, in-plane Sn-Se bonds (d_2) and the greater number of neighboring Sn-Se bonds of $SnSe_7$ enhance the vibrational frequencies of related Sn and Se atoms. The first TO phonons of both structures have relatively low frequencies at the zone center (~0.75 THz) and overlap with the acoustic branches, which indicates strong coupling between them. The phonon dispersions of the orthorhombic SnSe can be separated into two regions with each region possessing 12 branches, as can be clearly seen from the bipartite shape of its VDOS, while there is no similar separation in the rock salt phase. From Fig. 3 it is obvious that the rock salt SnSe exhibits an almost symmetric shape of the phonon dispersion

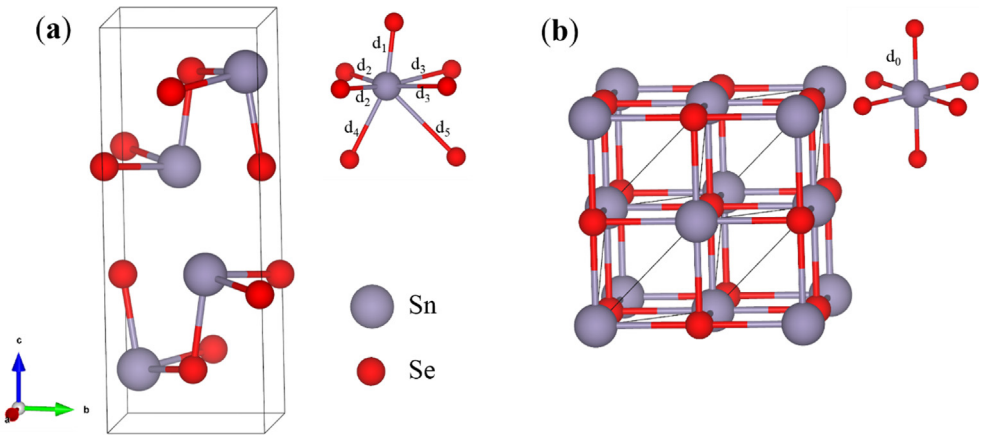

Fig. 1. Crystal structure of (a) the orthorhombic SnSe and (b) the rock salt SnSe. The solid line depicts the unit cell.

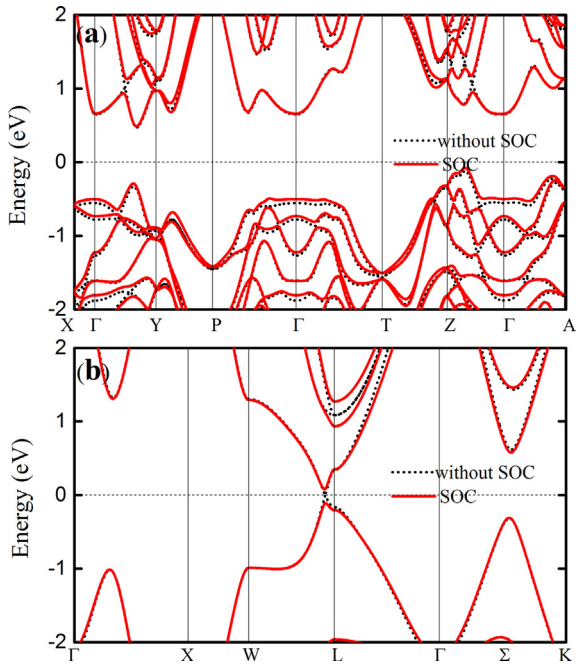

Fig. 2. Electronic band structure of (a) the orthorhombic SnSe and (b) the rock salt SnSe along some high-symmetry K-points in the irreducible Brillouin zone with and without SOC. The Fermi level was set to 0 eV. The implementation of SOC opens a gap of 0.19 eV around the L point in the rock salt SnSe.

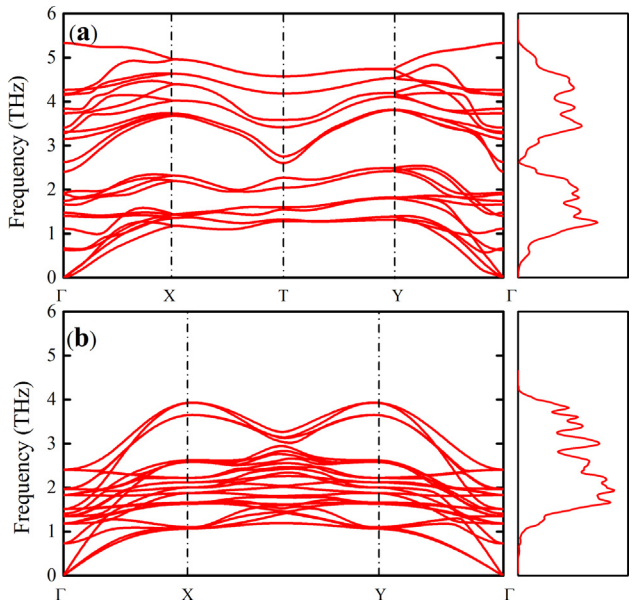

Fig. 3. The phonon dispersion curves along high-symmetry K-points in the irreducible Brillouin zone and the phonon vibrational density of states of (a) the orthorhombic SnSe and (b) the rock salt SnSe. The optical modes of the orthorhombic SnSe show larger values than those of the rock salt structure.

curves along the Γ-X and Γ-Y directions, while showing an asymmetric shape for the orthorhombic SnSe, especially for the low-frequency phonon modes. We present the frequency dependent phonon group velocities of both structures at 300 K in Fig. 4a. The average group velocities of low frequency phonons for both structures are comparable. While in the high frequency region, the rock salt SnSe shows a larger group velocity with most modes over 2000 m/s, it also corresponds to the highly dispersive optical phonons above 2 THz of the phonon spectrum (Fig. 3b).

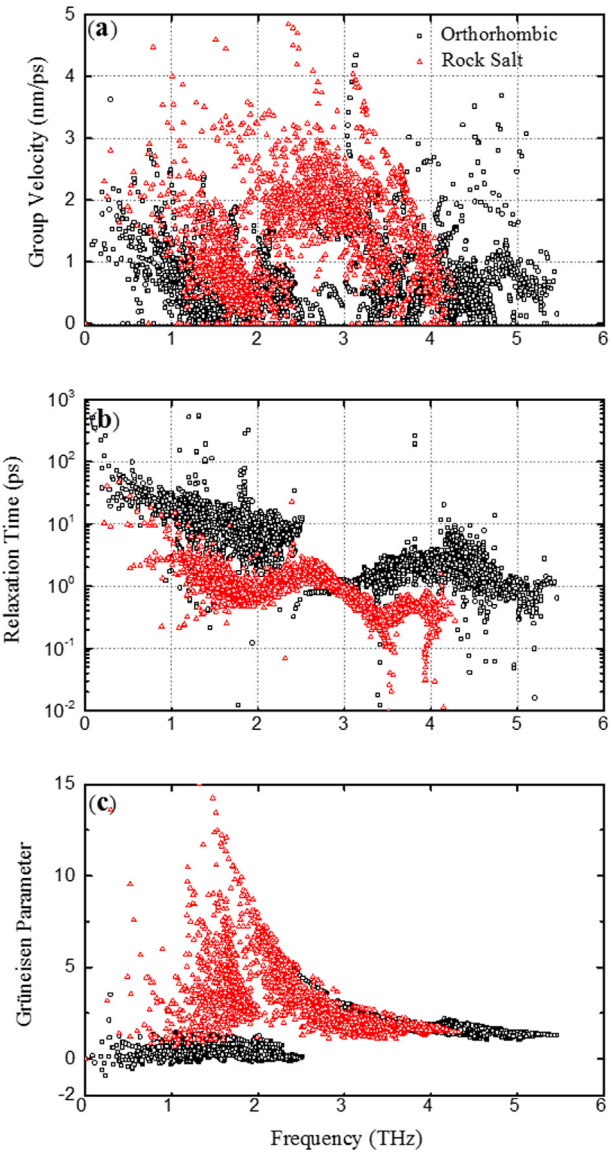

Fig. 4. Frequency dependent (a) phonon group velocity (b) phonon relaxation time and (c) Grüneisen parameter at 300 K of the orthorhombic (black) SnSe and the rock salt (red) SnSe. (For interpretation of the references to colour in this figure legend, the reader is referred to the web version of this article.)

The calculated κ_L of the rock salt SnSe is lower than the average κ_L of the orthorhombic SnSe between 300 K and 800 K, despite its higher crystal symmetry, as illustrated in Fig. 5. This is partly due to the lower phonon energy in the phonon spectrum. The κ_L of the orthorhombic SnSe shows distinctively anisotropic κ_L between the b and c directions, which can be traced back to the phonon spectrum: the phonon frequencies along Γ-Y are higher than along the Γ-X direction. The κ_L of the orthorhombic SnSe along the a, b, and c axes decreases from 0.8, 3.4, 2.6 W/m K at 300 K and to 0.3, 1.3, 1.0 W/m K as the temperature rises to 800 K. Although the calculated thermal conductivities of the orthorhombic phase depict much higher values compared to the experimental data [6], the corresponding magnitude sequence is in agreement (κ_b L > κ_c L > κ_a L). The surprisingly low κ_L of the single crystal SnSe measured in experiments might be caused by defects that are not considered in our calculations. The increasing temperature reduces the lattice thermal conductivity of the rock salt SnSe from 1.5 W/m K at 300 K to 0.58 W/m K at 800 K. Note that the κ_L < 0.6

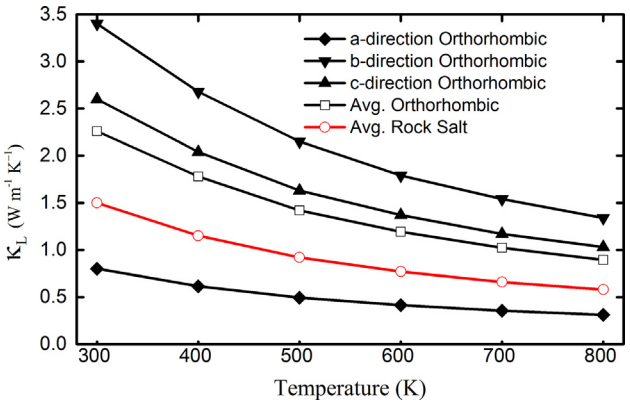

Fig. 5. Temperature dependent lattice thermal conductivity of the orthorhombic SnSe (black) and the rock salt SnSe (red). The average thermal conductivity of the rock salt structure is lower than that of the orthorhombic structure from 300 K to 800 K. (For interpretation of the references to colour in this figure legend, the reader is referred to the web version of this article.)

W/m K of the rock salt SnSe at 800 K is extremely small for such a high-symmetry crystalline solid. The essence of achieving record high zT in the orthorhombic SnSe comes down to the low κ_L, however, the even lower κ_L of the rock salt SnSe is then both surprising and of great significance, it also reveals the indecisive role the orthorhombic structure is playing in achieving low κ_L for SnSe. While the mechanism remains unclear, it is necessary for us to thoroughly analyze the thermal transport properties of the rock salt SnSe and compare them with the orthorhombic phase.

Substantial phonon anharmonicity was found in the rock salt SnSe, which leads to the reduction of κ_L. Fig. 4b plots the frequency dependent phonon relaxation times of both structures at 300 K. The phonon relaxation time of the rock salt SnSe is smaller in comparison with the orthorhombic phase, it is also shorter than those of many other bulk materials (~100 ps for PbTe [18], ~200 ps for CoSb3 [28] at f = 0.4 THz and T = 300 K). In particular, the relaxation time of most phonon branches of the rock salt SnSe is smaller than 10 ps, which is an indication of a large anharmonic effect. To further evaluate the anharmonicity, we calculated the Grüneisen parameters, which characterize the relationship between phonon frequency and crystal volume change and indicates the degree of anharmonicity of a structure. The Grüneisen parameter averaged over all phonons are 1.2 and 3.2 for the orthorhombic and the rock salt SnSe, respectively. The average Grüneisen parameter of the rock salt SnSe is larger than both that of the orthorhombic phase and most IV-VI TE materials [29,30]. The large Grüneisen parameter of the rock salt SnSe is also a reflection of its small relaxation time and hence the low lattice thermal conductivity. The Grüneisen parameters as a function of frequency at 300 K are illustrated in Fig. 4c, from which it is obvious that the rock salt SnSe has larger values compared with the orthorhombic structure especially around 2 THz. We also find long-range force-constant components along the [0 1 1] direction for the orthorhombic SnSe and along the [0 0 1] direction for the rock salt SnSe (Fig. 6a). This long-range interaction has been proven previously to account for the strong anharmonic phonon scattering [12,31]. For instance, as shown in Fig. 6a (red circles), the force-constants between the 2nd [0 0 1] neighbor (fourth-nearest neighbor) for the rock salt SnSe, spaced 6.06 Å apart along the [0 0 1] direction, are comparable to those of 1st [0 0 1] neighbor (nearest neighbor) and are much larger than the second- ([1 1 0] direction) and third-nearest ([1 1 1] direction) neighbor, which indicates a non-negligible long-range correlation in the [0 0 1] direction. It can also be considered as a long-range charge-density perturbation on atomic displacements as shown in Fig. 6b, where polarizations are extended along [0 1 1] and [0 0 1] for the orthorhombic and the rock salt SnSe, respectively. These long-range polarizations can be explained by the resonant bonding of p-states, where the bonding electrons can easily move in the p-orbitals of adjacent atoms, and are consistent with the insights that resonant bonding of chalcogenide p-states can lead to large Grüneisen parameters [31] and the reduction of the lattice thermal conductivity.

For the rock salt SnSe, the κ_L is dominated by the optical phonons, which is very different from the orthorhombic structure. We clarify the lattice thermal conductivity for both structures as a function of frequency in Fig. 7. The dashed black lines denote the acoustic cutoff. The most remarkable difference between the two structures is how much the acoustic phonons contribute to the lattice thermal conductivity. For instance, the acoustic phonons of the orthorhombic SnSe contribute nearly 70% of the κ_L (Fig. 7a), while the κ_L of the rock salt SnSe is dominated by the optical phonons. Even though the κ_L of the rock salt SnSe increases steadily throughout the acoustic region, the optical part accounts for an additional drastic increment between 2 and 3 THz (Fig. 7b), reducing the contribution of acoustic phonons to 23%. We can gain some insights about the thermal contributions from the relaxation time and group velocity analysis: the relaxation time of the orthorhombic SnSe above 3 THz (Fig. 4b) is smaller than below it, considering the close average group velocity below and above 3 THz, it is obvious that the lattice thermal conductivity is mostly due to the phonon branches below 3 THz. More importantly, the acoustic phonons below 1 THz yield the highest relaxation time, and are in this perspective playing a significant role in the thermal conductivity of the orthorhombic SnSe. For the rock salt SnSe, the relaxation time of the optical phonons (>1.5 THz) is comparable to the acoustic branches, thus the distinctively large values of group velocity above 2 THz, as shown in Fig. 4a, explains the rapid κ_L growth around 2–3 THz depicted in Fig. 7b. Given that for many bulk materials, the optical phonons hardly matter for the lattice thermal conductivity calculation, for instance, in bulk Si the optical phonons only accounts for about 5% of the lattice thermal conductivity [32], the findings of the small acoustic contribution to κ_L of the rock salt SnSe are rather intriguing. Moreover, the optical phonons provide important scattering channels for acoustic phonons and are essential for lowering the thermal conductivity. Assuming that the optical contribution to κ_L is completely suppressed by point-defect scattering in experiments, the κ_L of the rock salt SnSe at 300 K will be suppressed to 0.35 W/m K, which is extremely attractive for further TE applications.

Another important factor in understanding heat conduction is the mean free path (MFP) for phonons. Fig. 8 plots the cumulative lattice thermal conductivity with respect to the MFP for phonons at 300 K for the orthorhombic and the rock salt SnSe. Most of the heat carrying phonons in the orthorhombic phase have MFPs below tens of nanometers, thus making the grain boundaries of polycrystalline SnSe too big to reduce the thermal conductivity. As for the rock salt phase, phonons with MFPs smaller than 10 nm comprise 89% of the lattice thermal conductivity as the dot-dash blue lines depict. In other words, even if the interface back scattered all the ballistic phonons, the κ_L of the rock salt SnSe would only be reduced by 11% when the length scale of the rock salt SnSe is 10 nm. The very short MFPs indicates that it would be very difficult for the rock salt SnSe to further reduce κ_L by nanostructuring.

4. Summary and conclusion

We performed comprehensive first-principles calculations to predict the thermal transport properties of the rock salt SnSe and compared it with the orthorhombic SnSe. The band structure of

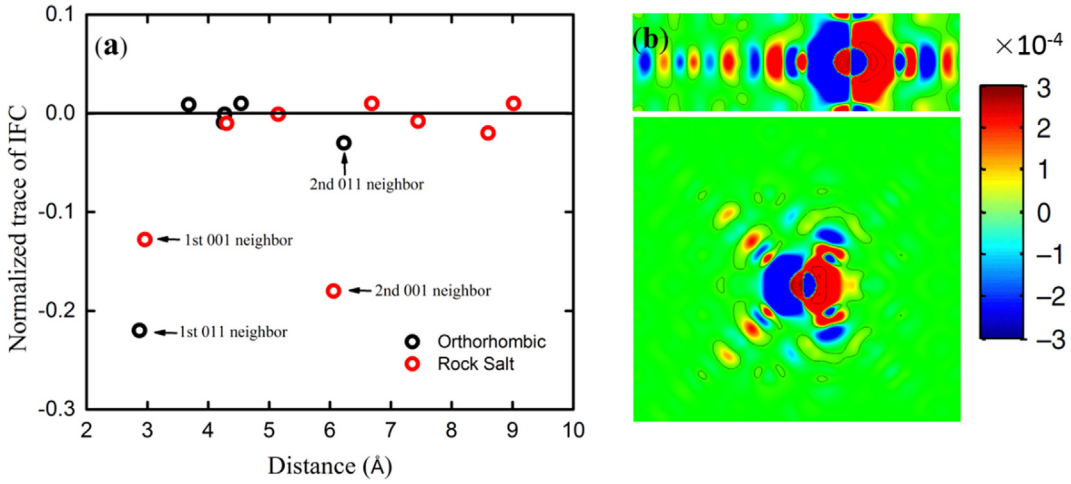

Fig. 6. (a) Normalized trace of interatomic force constant tensors versus atomic distances for the orthorhombic SnSe and the rock salt SnSe. The normalization is done by the trace value of self-interaction force constants [31]. (b) Electron density distribution change by the displacement of the center atom in the rock salt (upper) SnSe and the orthorhombic (lower) SnSe. Both structures show long-range force constant components and long-range charge density perturbations. The unit is $Å^{-4}$.

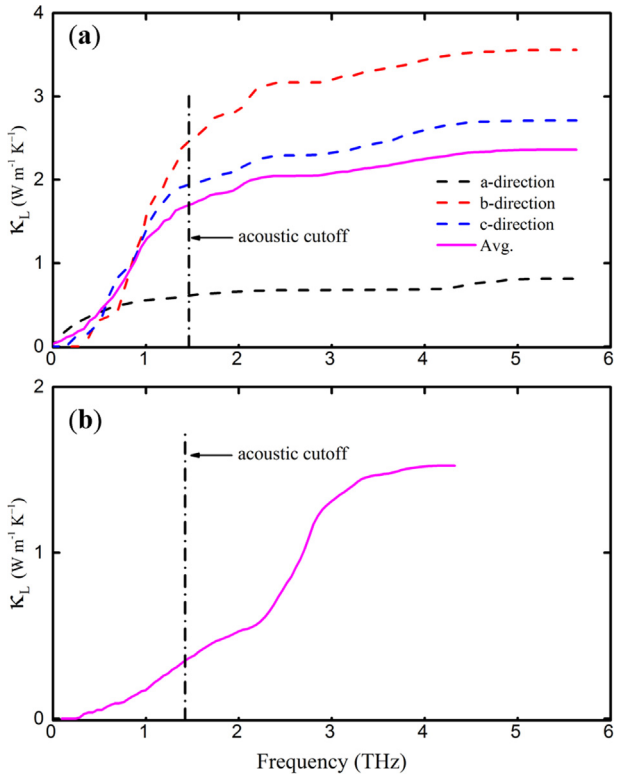

Fig. 7. The calculated lattice thermal conductivity with respect to the phonon frequency at 300 K for (a) the orthorhombic SnSe and (b) the rock salt SnSe. The black dot-dash denotes the acoustic cutoff. The thermal conductivity of the orthorhombic structure is dominated by the acoustic phonons, which is opposite that of the rock salt structure.

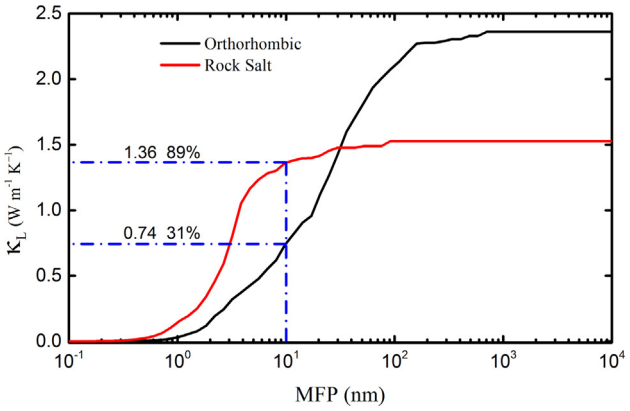

Fig. 8. Lattice thermal conductivity as a function of MFP for phonons at 300 K of the orthorhombic (black) and the rock salt (red) SnSe. The phonons with a MFP below 10 nm contribute 89% of the thermal conductivity for the rock salt structure. (For interpretation of the references to colour in this figure legend, the reader is referred to the web version of this article.)

the rock salt SnSe shows a small band gap of 0.19 eV with the implementation of the spin-orbit interaction. The phonon frequencies of the rock salt SnSe are qualitatively lower than those of the orthorhombic phase, and we used a simple bond length model to understand them. The thermal transport results reveal that the rock salt SnSe exhibits an extremely low κ_L compared to the orthorhombic phase through the whole temperature range we studied, for instance, 1.5 W/m K at 300 K. The small value of the phonon relaxation time of the rock salt SnSe indicates the existence of large anharmonicity, which is further clarified by the huge Grüneisen parameters and the prominent long-range force constants [31]. The contributions of κ_L from each phonon branch is further elaborated as well as its relationship with the phonon relaxation time and phonon group velocity. Different from the orthorhombic SnSe, the κ_L of the rock salt SnSe is mostly contributed by the optical phonons, which would effectively lower it to 0.35 W/m K at 800 K, assuming all optical contributions are eliminated by defects in experiments. The MFP analysis show that it is difficult to further reduce the κ_L of rock salt SnSe by nanostructuring. In light of these findings, we provide evidence that the orthorhombic structure plays an indecisive role for achieving low κ_L for SnSe. The comparative study of the rock salt and orthorhombic structured SnSe shows new insight in understanding the thermal properties. Finally, the even lower κ_L shows considerable potential for the rock salt SnSe to be used as a high performance TE or other thermal material.

Acknowledgements

This paper was partially supported by the National Natural Science Foundation of China, the Special Funds for Major State

Basic Research [Grant No. NCET-10-0351]. The Program for Professor of Special Appointment at Shanghai Institutions of Higher Learning, and the Research Program of Shanghai Municipality and the Ministry of Education.

References

[1] C. Harman, Quantum dot superlattice thermoelectric materials and devices, Science 297 (2002) 2229–2232, https://doi.org/10.1126/science.1072886.
[2] G.J. Snyder, E.S. Toberer, Complex thermoelectric materials, Nat. Mater. 7 (2008) 105–114, https://doi.org/10.1038/nmat2090.
[3] P. Heremans, V. Jovovic, S. Toberer, A. Saramat, K. Kurosaki, A. Charoenphakdee, S. Yamanaka, J. Snyder, Enhancement of thermoelectric of the electronic density of states, Science 321 (2008) 1457–1461, https://doi.org/10.1126/science.1159725.
[4] J.R. Sootsman, D.Y. Chung, M.G. Kanatzidis, New and old concepts in thermoelectric materials, Angew. Chem. – Int. Ed. 48 (2009) 8616–8639, https://doi.org/10.1002/anie.200900598.
[5] M. Zebarjadi, K. Esfarjani, M.S. Dresselhaus, Z.F. Ren, G. Chen, Perspectives on thermoelectrics: from fundamentals to device applications, Energy Environ. Sci. 5 (2012) 5147–5162, https://doi.org/10.1039/C1EE02497C.
[6] L.-D. Zhao, S.-H. Lo, Y. Zhang, H. Sun, G. Tan, C. Uher, C. Wolverton, V.P. Dravid, M.G. Kanatzidis, Ultralow thermal conductivity and high thermoelectric figure of merit in SnSe crystals, Nature 508 (2014) 373–377, https://doi.org/10.1038/nature13184.
[7] L.-D. Zhao, G. Tan, S. Hao, J. He, Y. Pei, H. Chi, H. Wang, S. Gong, H. Xu, V.P. Dravid, C. Uher, G.J. Snyder, C. Wolverton, M.G. Kanatzidis, Ultrahigh power factor and thermoelectric performance in hole-doped single-crystal SnSe, Science 351 (2016) 141–144, https://doi.org/10.1126/science.aad3749.
[8] P.B. Littlewood, The crystal structure of IV-VI compounds. I. Classification and description, J. Phys. C Solid State Phys. 13 (1980) 4855–4873, https://doi.org/10.1088/0022-3719/13/26/009.
[9] J. Carrete, N. Mingo, S. Curtarolo, Low thermal conductivity and triaxial phononic anisotropy of SnSe, Appl. Phys. Lett. 105 (2014) 101907, https://doi.org/10.1063/1.4895770.
[10] C.-L. Chen, H. Wang, Y.-Y. Chen, T. Day, G.J. Snyder, Thermoelectric properties of p-type polycrystalline SnSe doped with Ag, J. Mater. Chem. A 2 (2014) 11171–11176, https://doi.org/10.1039/C4TA01643B.
[11] S. Sassi, C. Candolfi, J.-B. Vaney, V. Ohorodniichuk, P. Masschelein, A. Dauscher, B. Lenoir, Assessment of the thermoelectric performance of polycrystalline p-type SnSe, Appl. Phys. Lett. 104 (2014) 212105, https://doi.org/10.1063/1.4880817.
[12] C.W. Li, J. Hong, A.F. May, D. Bansal, S. Chi, T. Hong, G. Ehlers, O. Delaire, Orbitally driven giant phonon anharmonicity in SnSe, Nat. Phys. 11 (2015) 1063–1069, https://doi.org/10.1038/nphys3492.
[13] R. Guo, X. Wang, Y. Kuang, B. Huang, First-principles study of anisotropic thermoelectric transport properties of IV-VI semiconductor compounds SnSe and SnS, Phys. Rev. B – Condens. Matter Mater. Phys. 92 (2015) 1–13, https://doi.org/10.1103/PhysRevB.92.115202.
[14] D. Bansal, J. Hong, C.W. Li, A.F. May, W. Porter, M.Y. Hu, D.L. Abernathy, O. Delaire, Phonon anharmonicity and negative thermal expansion in SnSe, Phys. Rev. B 94 (2016) 1–13, https://doi.org/10.1103/PhysRevB.94.054307.
[15] K. Peng, X. Lu, H. Zhan, S. Hui, X. Tang, G. Wang, J. Dai, C. Uher, G. Wang, X. Zhou, Broad temperature plateau for high ZTs in heavily doped p-type SnSe single crystals, Energy Environ. Sci. 9 (2016) 454–460, https://doi.org/10.1039/C5EE03366G.
[16] G. Qin, Z. Qin, W.-Z. Fang, L.-C. Zhang, S.-Y. Yue, Q.-B. Yan, M. Hu, G. Su, Diverse anisotropy of phonon transport in two-dimensional group IV–VI compounds: a comparative study, Nanoscale 8 (2016) 11306–11319, https://doi.org/10.1039/C6NR01349J.
[17] R.L. González-Romero, A. Antonelli, J.J. Meléndez, Insights into the thermoelectric properties of SnSe from ab initio calculations, Phys. Chem. Chem. Phys. 19 (2017) 12804–12815, https://doi.org/10.1039/C7CP01160A.
[18] Z. Tian, J. Garg, K. Esfarjani, T. Shiga, J. Shiomi, G. Chen, Phonon conduction in PbSe, PbTe, and PbTe1-xSex from first-principles calculations, Phys. Rev. B – Condens. Matter Mater. Phys. 85 (2012) 1–7, https://doi.org/10.1103/PhysRevB.85.184303.
[19] P.E. Blöchl, Projector augmented-wave method, Phys. Rev. B 50 (1994) 17953–17979, https://doi.org/10.1103/PhysRevB.50.17953.
[20] G. Kresse, D. Joubert, From ultrasoft pseudopotentials to the projector augmented-wave method, Phys. Rev. B 59 (1999) 1758–1775, https://doi.org/10.1103/PhysRevB.59.1758.
[21] G. Kresse, J. Furthmüller, Efficiency of ab-initio total energy calculations for metals and semiconductors using a plane-wave basis set, Comput. Mater. Sci. 6 (1996) 15–50, https://doi.org/10.1016/0927-0256(96)00008-0.
[22] G. Kresse, J. Furthmüller, Efficient iterative schemes for *ab initio* total-energy calculations using a plane-wave basis set, Phys. Rev. B 54 (1996) 11169–11186, https://doi.org/10.1103/PhysRevB.54.11169.
[23] J.P. Perdew, K. Burke, M. Ernzerhof, Generalized gradient approximation made simple, Phys. Rev. Lett. 77 (1996) 3865–3868, https://doi.org/10.1103/PhysRevLett. 77.3865.
[24] A. Togo, I. Tanaka, First principles phonon calculations in materials science, Scr. Mater. 108 (2015) 1–5, https://doi.org/10.1016/j.scriptamat.2015.07.021.
[25] W. Li, J. Carrete, N.A. Katcho, N. Mingo, ShengBTE: a solver of the Boltzmann transport equation for phonons, Comput. Phys. Commun. 185 (2014) 1747–1758, https://doi.org/10.1016/j.cpc.2014.02.015.
[26] J.M. Skelton, S.C. Parker, A. Togo, I. Tanaka, A. Walsh, Thermal physics of the lead chalcogenides PbS, PbSe, and PbTe from first principles, Phys. Rev. B – Condens. Matter Mater. Phys. 89 (2014) 1–10, https://doi.org/10.1103/PhysRevB.89.205203.
[27] Y. Pei, X. Shi, A. Lalonde, H. Wang, L. Chen, G.J. Snyder, Convergence of electronic bands for high performance bulk thermoelectrics, Nature 473 (2011) 66–69, https://doi.org/10.1038/nature09996.
[28] R. Guo, X. Wang, B. Huang, Thermal conductivity of skutterudite $CoSb_3$ from first principles: substitution and nanoengineering effects, Sci. Rep. 5 (2015) 1–9, https://doi.org/10.1038/srep07806.
[29] S. Bozin, D. Malliakas, P. Souvatzis, T. Proffen, A. Spaldin, G. Kanatzidis, L. Billinge, Entropically stabilized local dipole formation in lead chalcogenides, Science 330 (2010) 1660–1663, https://doi.org/10.1126/science.1192759.
[30] L.-D. Zhao, C. Chang, G. Tan, M.G. Kanatzidis, SnSe: a remarkable new thermoelectric material, Energy Environ. Sci. 9 (2016) 3044–3060, https://doi.org/10.1039/C6EE01755J.
[31] S. Lee, K. Esfarjani, T. Luo, J. Zhou, Z. Tian, G. Chen, Resonant bonding leads to low lattice thermal conductivity, Nat. Commun. 5 (2014) 1–8, https://doi.org/10.1038/ncomms4525.
[32] K. Esfarjani, G. Chen, T. Stokes, Heat transport in silicon from first-principles calculations, Phys. Rev. B – Condens. Matter Mater. Phys. 84 (2011) 1–11, https://doi.org/10.1103/PhysRevB.84.085204.